Energy Budget of Nonlinear Internal Waves near Dongsha

Ren-Chieh Lien
Applied Physics Laboratory
University of Washington
Seattle, Washington 98105
phone: (206) 685-1079 fax: (206) 543-6785 email: lien@apl.washington.edu

LONG-TERM GOALS

Our long-term scientific goal is to understand the mechanisms by which mixing occurs in the ocean and thereby help develop improved parameterizations of mixing for ocean models. Mixing within the stratified ocean is our particular focus as the complex interplay of internal waves from a variety of sources and turbulence makes this a current locus of uncertainty. In this study, our broad focus is on the energy sources of nonlinear internal waves (NLIWs) in a complex environment of strong internal tides and abrupt topography (continental shelf and slope). We expect a rapid evolution of internal tides and NLIWs, and we aim to understand their dynamics, energy cascade, and role in mixing.

OBJECTIVES

The primary objectives of the present project are 1) to identify the generation site and understand the generation mechanism of NLIWs, 2) to understand the evolution of NLIWs interacting with abrupt topography, 3) to quantify the energy budget and energy cascade from internal tides to NLIWs, and 4) to quantify the seasonal variation of the energy of NLIWs near Dongsha Island in the northern South China Sea (SCS). Our particular interest is to understand the energy cascade from barotropic tides, internal tides, and NLIWs to turbulence mixing in the northern SCS, and to understand the evolution of NLIWs interacting with the shoaling continental slope.

APPROACH

Our approach is to take direct observations of NLIWs near Dongsha Island where NLIW are often captured in satellite images. Primary platforms include an ADV Lagrangian Float, a bottom mounted ADCP mooring array, shipboard EK500, marine radar, ADCP, and CTD. Our main goals are to quantify the energy budget and evolution of NLIWs across the rapidly shoaling continental slope and the gentle plateau near Dongsha Island and to exploit and quantify the seasonal variation of the NLIW characteristics.

WORK COMPLETED

We have completed three components of this observational experiment: (1) pilot observations in 2005, (2) extended observations in 2006–2007, and (3) intensive observations in 2007.

Report Documentation Page		Form Approved OMB No. 0704-0188

1. REPORT DATE **30 SEP 2008**	2. REPORT TYPE **Annual**	3. DATES COVERED **00-00-2008 to 00-00-2008**
4. TITLE AND SUBTITLE **Energy Budget Of Nonlinear Internal Waves Near Dongsha**		5a. CONTRACT NUMBER
		5b. GRANT NUMBER
		5c. PROGRAM ELEMENT NUMBER
6. AUTHOR(S)		5d. PROJECT NUMBER
		5e. TASK NUMBER
		5f. WORK UNIT NUMBER
7. PERFORMING ORGANIZATION NAME(S) AND ADDRESS(ES) **University of Washington,Applied Physics Laboratory,Seattle,WA,98105**		8. PERFORMING ORGANIZATION REPORT NUMBER
9. SPONSORING/MONITORING AGENCY NAME(S) AND ADDRESS(ES)		10. SPONSOR/MONITOR'S ACRONYM(S)
		11. SPONSOR/MONITOR'S REPORT NUMBER(S)

12. DISTRIBUTION/AVAILABILITY STATEMENT
Approved for public release; distribution unlimited

13. SUPPLEMENTARY NOTES
code 1 only

14. ABSTRACT

Our long-term scientific goal is to understand the mechanisms by which mixing occurs in the ocean and thereby help develop improved parameterizations of mixing for ocean models. Mixing within the stratified ocean is our particular focus as the complex interplay of internal waves from a variety of sources and turbulence makes this a current locus of uncertainty. In this study, our broad focus is on the energy sources of nonlinear internal waves (NLIWs) in a complex environment of strong internal tides and abrupt topography (continental shelf and slope). We expect a rapid evolution of internal tides and NLIWs, and we aim to understand their dynamics, energy cascade, and role in mixing.

15. SUBJECT TERMS

16. SECURITY CLASSIFICATION OF:			17. LIMITATION OF ABSTRACT	18. NUMBER OF PAGES	19a. NAME OF RESPONSIBLE PERSON
a. REPORT **unclassified**	b. ABSTRACT **unclassified**	c. THIS PAGE **unclassified**	**Same as Report (SAR)**	**21**	

Pilot Observations (April 2005)

In April 2005, we conducted a two-week observational experiment near Dongsha. Large-amplitude NLIWs, greater than 150 m, and strong turbulence mixing were observed by the Lagrangian float and shipboard sensors including ADCP, CTD, EK500, and X-band marine radar. Combined remote sensing and in-situ measurements provided detailed properties of large-amplitude NLIWs.

Extended ADCP Observations (June 2006–May 2007)

An array of three ADCP moorings was deployed along the prevailing path of NLIWs near Dongsha in June 2006. Three ADCPs were serviced once and recovered in May 2007. Two of three moorings took velocity measurements for about 11 months. These long-term observations of NLIWs allow us to (1) quantify the seasonal variation of NLIW energy, (2) map the geographical distribution, (3) better understand the dynamics of NLIW evolution over the shoaling topography, and (4) assess the model prediction skill of NLIWs.

Intensive Observations (April–May 2007)

We participated in the multi-ship intensive observation experiment near Dongsha in April–May 2007. Our main goals were to understand the interaction of internal waves, including internal tides and NLIWs, with the rapidly shoaling continental slope, and to quantify the energy budget of internal waves near Dongsha. Our primary instruments included Scripps Institution's fast CTD profiler, and shipboard ADCP, CTD, EK500, and marine radar. During the cruise, two McLane moored profilers were deployed, one on the continental slope and the other on the Dongsha plateau (Fig. 2).

In 2007–2008 we began processing CTD and ADCP data collected during the intensive observations in April–May 2007, and processing ADCP data taken in the extended mooring observations on the slope of Dongsha Plateau, June 2006–May 2007. Our main focus in 2008 is to develop schemes to compute (1) the total kinetic energy of NLIWs, (2) the propagation speed and direction of NLIWs, and (3) the potential energy of NLIWs using moored ADCP data. The kinetic energy of NLIWs is measured directly by moored ADCP (Fig. 18).

The average wave speed between moorings may be estimated by the difference of arrival times of NLIWs on moorings across the Dongsha Plateau. The extrapolation of the wave speed to individual mooring site could be seriously inaccurate because NLIWs reduce propagation speed dramatically over the shoaling slope across three moorings. Therefore, it is necessary to develop independent schemes to estimate propagation velocity, using ADCP measurements at individual mooring sites to compute the NLIW energy flux at mooring sites. We have developed the scheme and confirmed our method using theoretical internal solitary wave solutions.

RESULTS

Bio-Physical Coupling: Pilot Whales Following NLIWs in SCS

Schools of pilot whales were observed behind the large-amplitude NLIWs. Moore and Lien (2007) proposed that prey availability for pilot whales in the SCS is influenced by the aggregative properties of NLIWs. This is the first report of cetaceans associated with internal waves. We expect that the ecosystem in the SCS is strongly modulated by NLIWs.

Shoaling NLIW: Trapped Core and Fission Process

In April 2005 large-amplitude NLIWs with the vertical displacement of more than 150 m appeared diurnally during the spring tide (Fig. 3). Within NLIWs, we found ~75-m of turbulent overturning (Fig. 4b). Trains of NLIWs appeared on the Dongsha plateau and evolved rapidly as they propagated westward into the shallower water (Fig. 4a).

On April 28 we followed an NLIW with the vertical displacement of ~170 m propagating westward from the upper continental slope (Fig. 5). At the third encounter, a second wave appeared behind the leading NLIW. The second NLIW had a smaller vertical displacement and propagated slower than the leading NLIW.

The NLIW evolved rapidly while propagating up the continental slope (Fig. 6). At the first encounter, the maximum westward current velocity U_{max} was nearly equal to the propagation speed C, 2 m s^{-1}. Propagating onto the continental slope, the NLIW wave speed decreased dramatically from 2 m s^{-1} to 1.2 m s^{-1} in 3.5 hr within 20 km, whereas the maximum westward current velocity remained at 2 m s^{-1}. The Froude number, $Fr = U_{max} / C$, was greater than one, suggesting the presence of a re-circulating core within the NLIW, confirmed by the shipboard ADCP velocity and the derived stream lines (Fig. 7). The trapped core had a ~100-m vertical scale, and ~500-m horizontal scale containing two counter rotating vortices (closed streamlines).

The zonal velocity averaging within the trapped core should be equal to the wave propagation speed. Assuming the meridional extent of NLIW of 10 km, the net mass transport of the trapped core is ~2 Sv. The trapped core propagates for ~30 km (Fig. 6) and causes significant transient mass transport in the SCS. The development of the trailing wave is shown in Fig. 7. We hypothesize that this fission process is triggered by the dissipative trapped core. Because of the strong turbulence mixing, water particles within the trapped core fail to make the complete loop, fall behind the trapped core, and form the second wave.

We compared properties of observed NLIWs with solutions of the fully nonlinear steady-state non-dissipative internal solitary wave model described by Dubriel–Jacotin–Long (DJL) (Fig. 8). The NLIW observed at the first encounter, before the formation of the trapped core, agrees well with the DJL solution. Observations taken after the first encounter do not agree with the DJL solutions. This is not unexpected because of the strong unsteadiness and dissipation within the NLIW. Interestingly, all observations during the first five encounters agree with the DJL solution at the first encounter. Collaborations with small-scale numerical modelers will be necessary to understand the dynamics of the shoaling NLIWs, the trapped core formation, and the fission process.

Radar Detection of NLIW Properties

Surface waves are modulated by NLIWs. In the SCS the interaction is extremely strong due to the large horizontal velocity convergence of NLIWs (Chang et al., 2008). Photos taken on a calm day during the experiment show a sequence of calm sea surface, breaking surface waves, isotropic surface waves, and boils during the passage of the NLIW during a calm day (Fig. 9). The shipboard marine radar reveals the strongest scattering strength corresponding to the strongest horizontal velocity convergence measured by the shipboard ADCP (Fig. 9b and 9c).

A composite view of the sea surface scattering strength, the horizontal velocity convergence and the vertical displacement of NLIWs (Fig. 10) shows the strongest surface scattering strength at the front portion of the NLIW, ~0.5 $\lambda_{\eta/2}$, where $\lambda_{\eta/2}$ is the wave-width at half of the maximum amplitude.

An empirical formula between the surface scattering strength and horizontal velocity convergence (Fig. 11) shows a linear relation at low horizontal velocity convergence that reaches an asymptotic value at high horizontal velocity convergence, indicating a saturation state presumably due to breaking surface waves. Following the power-law and the linear fits between the scattering strength and the local wind speed, the maximum surface scattering enhancement by NLIWs is equivalent to that caused by a wind of ~6 m s^{-1} with surface waves of ~1.5 m, according to the Beaufort wind scale. In other words, the surface scattering enhancement induced by NLIWs will be overwhelmed by that induced by the wind and cannot be identified with the X-band radar when the wind is stronger than 6 m s^{-1}. The vertical displacement of NLIWs is found to be proportional to the spatial integration of the surface scattering strength (not shown). Our analysis concludes that in the low-wind condition remote sensing measurements may provide useful predictions of horizontal velocity convergences, amplitudes, and spatial structures of NLIWs. Further applications and modification of our empirical formulas in different conditions of wind speed, surface waves, and NLIWs, or with other remote sensing methods should be investigated.

Rapid Evolution of Shoaling NLIWs Revealed by Mooring Array

Our long-term moored ADCP velocity observations reveal a complex pattern of energy evolution across three mooring sites (Fig. 12). These examples show (1) a monotonic decrease of NLIW energy from LR1 to LR3, (2) an increase of NLIW energy at LR2, and (3) an increase of NLIW energy at LR3. Cases (1) and (2) are typical. The fourth case shows the development of a wave train between LR2 and LR3.

At LR1, the maximum westward horizontal velocity U_{max} within the NLIW is always smaller than the propagation speed C, suggesting the absence of a trapped core (Fig. 15). At LR2, nearly 40% of NLIWs have $U_{max} > C$, suggesting the presence of trapped cores. Apparently, trapped cores are formed when NLIWs propagate from LR1 to LR2, within a short distance of ~9 miles.

Seasonal Variations of NLIW Properties

Long-term moored observations reveal seasonal variations of the arrival time (Fig. 16), the propagation speed (Fig. 17), and the total kinetic energy of NLIWs (Fig. 18). In spring, NLIWs arrive at LR1 nearly the same time every day and once a day, except occasional weaker NLIWs in the early morning, consistent with observations in the pilot experiment. In January–Feburary 2007, only a few weak NLIWs were observed. During the rest of the year, two distinct groups of NLIWs arrive at the mooring site at different times of the day. From mid June to November, the arrival time shows a ~40-min delay every day.

Averaging over ~1-year of observations, the total kinetic energy of NLIWs decreases westward from LR1 to LR3 (Fig. 13a). Comparing the total kinetic energy of individual waves from LR1 to LR3 (Fig. 14) suggests that (1) strong NLIWs at LR1 lose energy before arriving at LR2, (2) weak NLIWs at LR1 gain energy before arriving at LR2, and (3) NLIWs mostly lose energy when propagating from LR2 to LR3. Note that the loss of energy may be due to either the dissipation process or the fission process.

Generation Region of Trapped-Core NLIWs

The rapid decrease of the propagation speed of NLIWs on the shoaling continental slope may lead to the formation of the trapped core, as observed in the 2005 pilot experiment (Fig. 6). Our long-term moored ADCP measurements show that the average propagation speed of NLIWs decreases from 2 m s^{-1} at LR1 to 1.8 m s^{-1} at LR2, and 1.3 m s^{-1} at LR3 (Fig. 13), consistent with observations in the pilot experiment (Fig. 6).

The propagation speed of NLIWs increases from June to October 2006, drops in November 2006, and remains at a low speed thereafter (Fig. 17). This pattern is robust at all three mooring sites. The vertical kinetic energy of NLIWs has a general decreasing trend from June to Dec. 2006 (Fig. 18), is the weakest in January–Feburary 2007, and increases in spring 2007.

Estimating NLIW Propagation Direction using Moored ADCP

Moored ADCP data provide vertical profiles of three components of velocity. The propagation direction of NLIW is the same as the major axis of the horizontal velocity. The estimation is illustrated by a NLIW event of May 2, 2007 (Figs. 19 and 20). The background flow field is computed by averaging observed velocity profiles within a time interval, ~ 20 minutes, before the arrival of NLIW (black box in Figure 19). Streamlines are computed by the time integration of the observed vertical velocity (white curves). The NLIW velocity field is computed by subtracting the background flow from the observed velocity field following the streamlines. The wave propagation direction is computed as the major axis of the NLIW horizontal velocity (Figure 20b). In this case, the linear least square fit suggests the wave propagation direction is $158° \pm 1°$ counterclockwise from the east. It is in good agreement with the estimate of the propagation direction, 157°, computed using the surface scattering intensity induced by the surface manifestation of NLIWs detected by the marine radar. Figure 20c shows the propagation direction estimated using the total horizontal velocity field, i.e., without subtracting the background velocity field. It is biased and has a larger uncertainty.

Estimation of NLIW Propagation Speed using Moored ADCP

Typically, NLIWs propagate across the mooring in 20 minutes. The propagation speed can be computed as

$$C = \frac{-\partial u / \partial t}{\partial w / \partial z} \quad , \tag{1}$$

where u is the horizontal velocity in the propagation direction assuming the C remains constant when propagating past the mooring.

To verify our method, we applied it to a set of solutions of nonlinear theoretical internal solitary waves produced by the DJL equation. Figure 21 illustrates the simulation of DJL internal solitary waves with a wave speed of -2 m s^{-1} using the observed stratification profile. The wave propagation speed is reproduced using (1), as expected, when using model results at the model resolution, 15-s time interval and 2-m vertical interval. After averaging model results within a time interval of 90 s and vertical interval of 16 m, corresponding to our mooring observations, the propagation speed computed using (1) is still within 10% of the true value.

We investigated the effect of ADCP noise by adding 4 cm s^{-1} random noise to the DJL solution (figure 22). The propagation speed of NLIW computed using (1) is -1.57 m s^{-1}, which is about 20% less than the true propagation speed. We are investigating a better scheme to reproduce the true propagation speed.

Figure 23 illustrates the application of (1) to velocity measurements of an NLIW event taken from a bottom mounted ADCP. Streamlines are computed from the time integration of the observed vertical velocity profile. The background velocity is removed from the observed velocity following streamlines. The wave propagation speed computed using (1) is -2.29 ± 0.18 m s^{-1}. The uncertainty is similar to that of DJL solutions after adding 4 cm s^{-1} random noise.

We will apply this method to all observed NLIWs and compare results with available observations of wave propagation speed from marine radar.

IMPACT/APPLICATION

Our analysis concludes that NLIWs evolve rapidly across the upper flank of the continental slope and the Dongsha plateau via complicated processes, e.g., the formation of trapped cores, and the development of wave trains. These processes are responsible for the strong dissipation of NLIWs in the SCS. Our analysis of combined remote sensing and in-situ measurements yields a model to predict NLIW properties applicable to satellite observations. The newly developed scheme to estimate NLIW wave speed and direction is useful for quantifying the wave property, including energy flux, using a single bottom mounted ADCP. Further long-term observations of NLIWs in the vicinity of Dongsha plateau are in progress and will provide a better prediction of NLIWs in the SCS.

RELATED PROJECTS

Study of Kuroshio Intrusion and Transport using Moorings, HPIES and EM-APEX Floats (N00014-08-1-0558) as a part of QPE DRI:

The primary objectives of this observational program are 1) to quantify and to understand the dynamics of the Kuroshio intrusion and its migration into the southern East China Sea (SECS), 2) to identify the generation mechanisms of the Cold Dome often found on the SECS, 3) to quantify the internal tidal energy flux and budgets on the SECS and study the effects of the Kuroshio front on the internal tidal energy flux, 4) to quantify NLIWs and provide statistical properties of NLIWs on the SECS , and 5) to provide our results to acoustic investigators to assess the uncertainty in acoustic predictions. Results of the NLIWI DRI will provide a better understanding of the dynamics of NLIWs that have strong effects on acoustic propagation and sonar performance.

Process Study of Oceanic Responses to Typhoons using Arrays of EM-APEX Floats and Moorings (N00014-08-1-0560) as a part of ITWP DRI:

We will study the dynamics of the oceanic response to and recovery from tropical cyclones in the western Pacific using long-term mooring observations and an array of EM-APEX floats. Pacific typhoons may cause cold pools on the continental shelf of the East China Sea.

REFERENCES

Chang, M.-H., R.-C. Lien, T. Y. Tang, Y. J. Yang, and J. Wang, A composite view of surface Signatures and interior properties of nonlinear internal waves: Observations and applications., *J. Atmos. Ocean. Technol.*, **25**, 1218-1227, 2008.

Chang, M.-H., R.-C. Lien, T. Y. Tang, E. A. D'Asaro, and Y. J. Yang, Energy flux of nonlinear internal waves in northern South China Sea, *Geophys. Res. Lett.*, **33,** L03607, doi:10.1029/2005GL025196, 2006.

Lien, R.-C., T. Y. Tang, M. H. Chang, E. A. D'Asaro, Energy of nonlinear internal waves in the South China Sea, *Geophys. Res. Lett.*, **32**, L05615, doi:10.1029/2004GL022012, 2005.

Moore, S. E., and R.-C. Lien, Pilot whales follow internal solitary waves in the South China Sea, *Mar. Mamm. Sci.*, **23**, 1, 193–196, 2007.

Zhao, Z., V. Klemas, Q. Zheng, and X.-H. Yang, Remote sensing evidence for baroclinic tide origin of internal solitary waves in the northeastern South China Sea, *Geophys. Res. Lett.*, **31**, L06302, doi:10,1029/2003GL019077, 2004.

PUBLICATIONS

Lien, R.-C., T. Y. Tang, M. H. Chang, E. A. D'Asaro, Energy of nonlinear internal waves in the South China Sea, *Geophys. Res. Lett.*, **32**, L05615, doi:10.1029/2004GL022012, 2005.

Chang, M.-H., R.-C. Lien, T. Y. Tang, E. A. D'Asaro, and Y. J. Yang, Energy flux of nonlinear internal waves in northern South China Sea, *Geophys. Res. Lett.*, **33**, L03607, doi:10.1029/2005GL025196, 2006.

Moore, S. E., and R.-C. Lien, Pilot whales follow internal solitary waves in the South China Sea, *Mar. Mamm. Sci.*, **23**, 1, 193–196, 2007.

Chang, M.-H., R.-C. Lien, T. Y. Tang, Y. J. Yang, and J. Wang, A composite view of surface signatures and interior properties of nonlinear internal waves: Observations and applications., *J. Atmos. Ocean. Technol.*, **25**, 1218-1227, 2008.
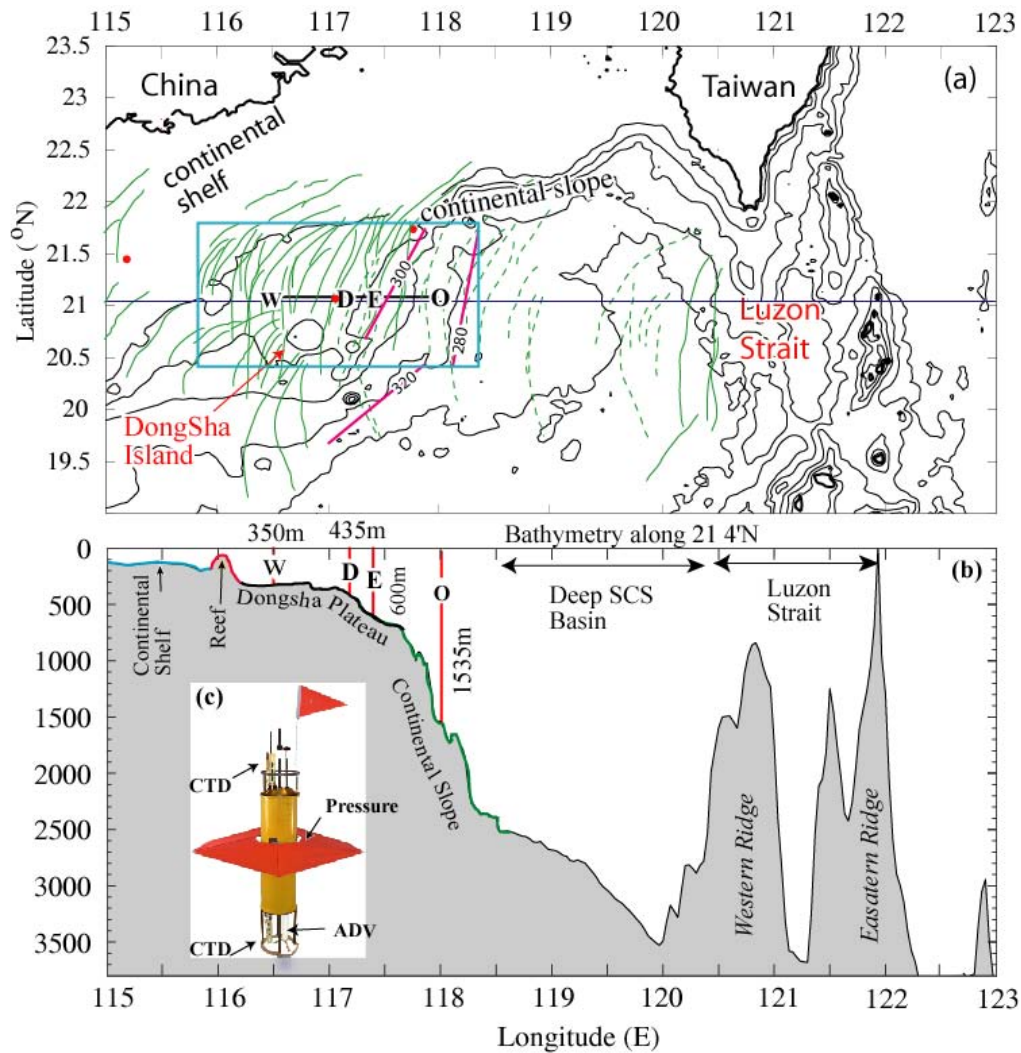
Figure 1: (a) Map of the northern South China Sea, and (b) bottom bathymetry along 21•4'N. In (a) green curves represent surface signatures of NLIWs identified in satellite images (Zhao et al., 2004), dashed for single-depression waves and solid for multiple wave packets. The blue box delineates the area where multiple wave packets are mostly found. Four primary stations in our April–May 2005 cruise are labeled as O, E, D and W. Shipboard and float measurements were taken along O-E-D-W. Three magenta curves illustrate isobaric orientations on the continental slope. In panel (b) two submarine ridges in the Luzon Strait are labeled. They are responsible for generating strong internal tides. Depths at four primary stations are also labeled. The inset (c) shows the Lagrangian float and sensors equipped on the float.
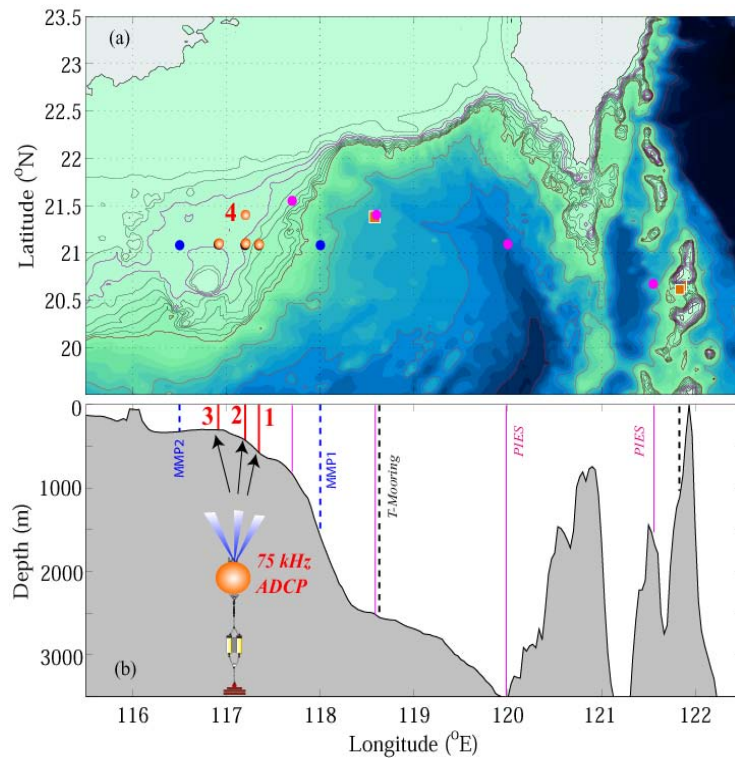
Figure 2: (a) Map of South China Sea and (b) bathymetry along 21 °N. Four yellow bullets and red lines mark the locations of moored ADCPs. The configuration of the bottom mounted 75-kHz ADCP is shown in (b). Two blue dots (vertical blue dashed lines), magenta dots (vertical magenta lines), and brown squares (vertical black dashed lines) mark the positions of McLane moored profilers (Alford), PIES (Farmer), and temperature moorings (Tang and Ramp), respectively. Labels 1–4 represent the moored ADCPs.
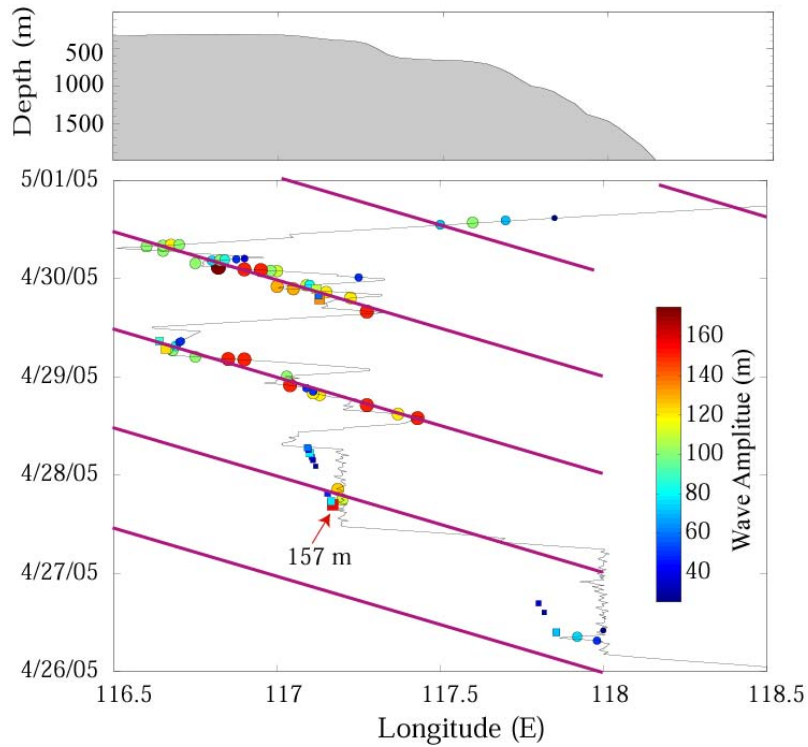
Figure 3: Compilation of amplitudes of NLIWs recorded on EK500 (color dots), shipboard ADCP, and Lagrangian float (filled squares). Colors and sizes of symbols represent amplitudes of NLIWs. The black curve indicates the ship track. Magenta curves illustrate the constant phase lines of observed NLIWs. NLIWs arrive diurnally.
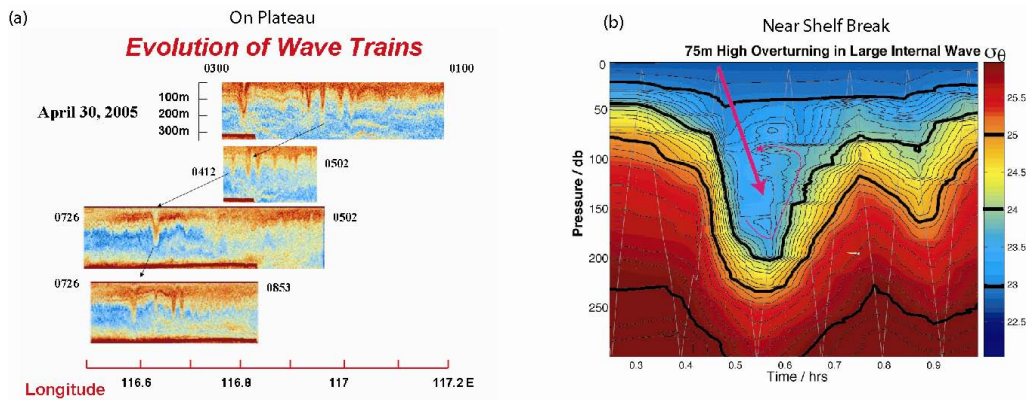
Figure 4: (a) Four sequential sections of EK500 images taken north of Dongsha Island illustrating the evolution of trains of NLIWs, and (b) contour of isopycnal surfaces taken with yoyo CTD profiles illustrating the large-amplitude NLIWs and large turbulence overturning. These observations were taken onboard of Taiwanese R/V Ocean Research 3 in April 2005. In panel (a) the beginning and end times of each section of EK500 image are labeled.

10
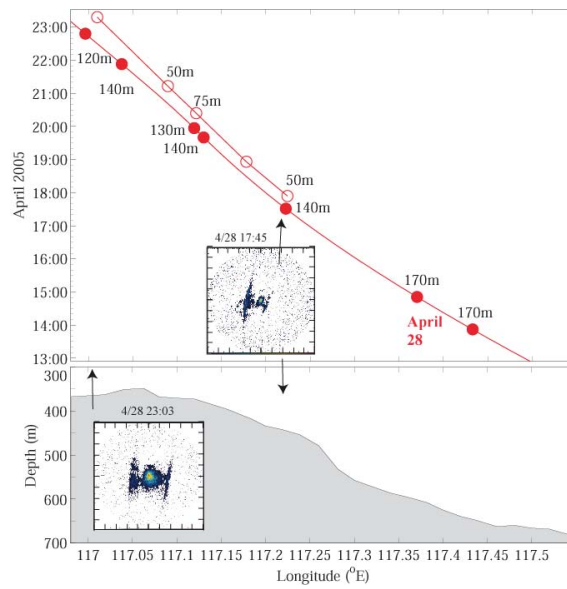
Figure 5: Tracking the evolution of a large-amplitude NLIW. Solid red dots in the upper panel show the locations and time of the tracked NLIW and open circles show the trailing wave, presumably developed from the tracked NLIW. Vertical amplitudes of NLIWs are labeled. Two insets are shipboard marine radar images showing the presence of two waves.
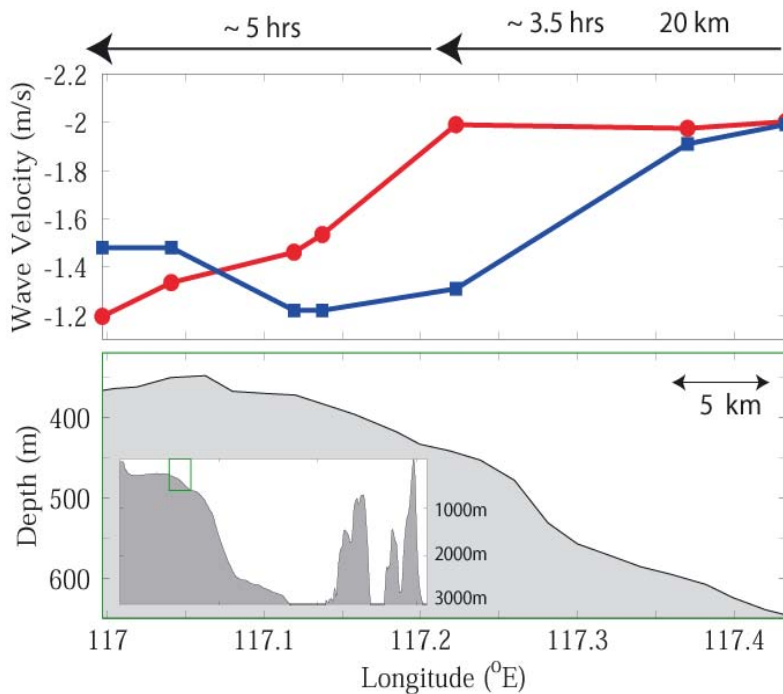
Figure 6: Evolution of maximum current velocity and propagation speed of a NLIW on shoaling topography. The upper panel shows the maximum westward zonal velocity (red curve) and the propagating speed of NLIW (blue curve). The bottom panel shows the bathymetry. The inset is the bathymetry along 21 °N in the SCS. A spatial scale of 5 km is shown.
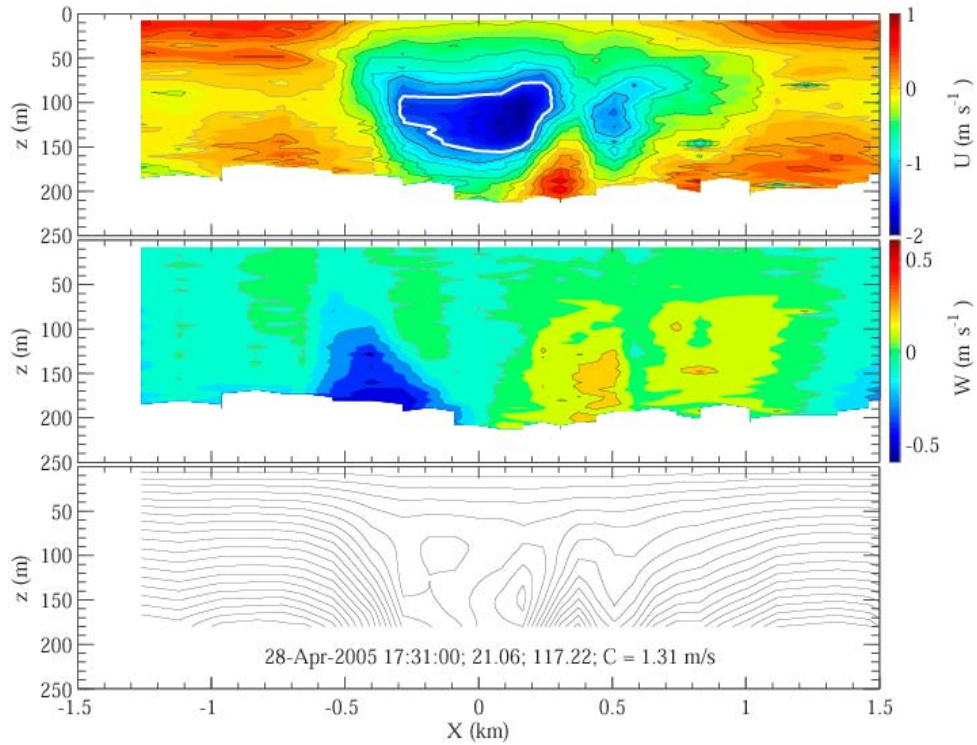
Figure 7: Illustration of the recirculation trapped core. The top two panels are contour plots of zonal velocity and vertical velocity observed by the shipboard ADCP during the third encounter with the NLIW (Figs. 5 and 6). The bottom panel shows the streamline computed from the zonal velocity. The white curve in the top panel marks the contour line of the westward propagation speed of the NLIW.
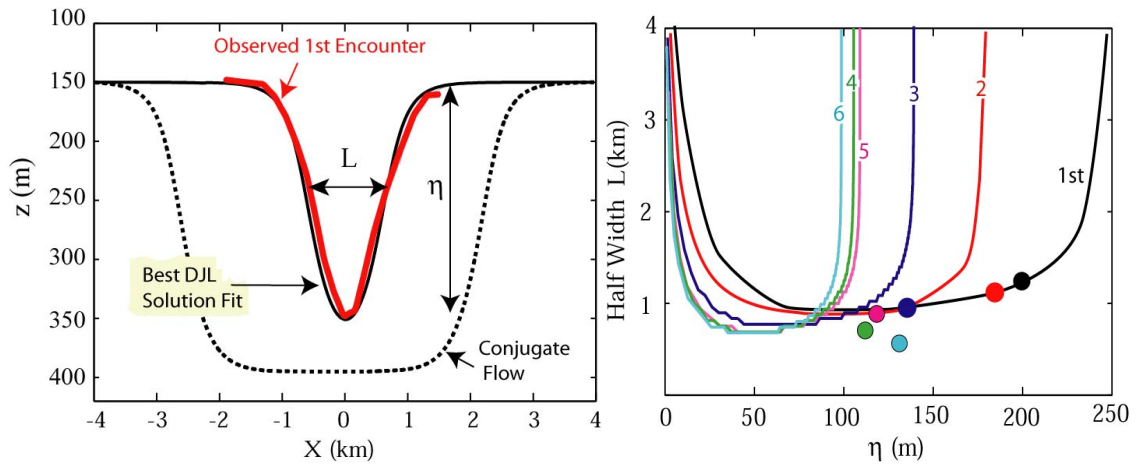
Figure 8: Observations compared with solutions of the Dubreil-Jacotin-Long (DJL) model. The left panel shows the good agreement between observations (red curve) at the first encounter and DJL (solid black curve). The right panel shows the comparison for observations in the first six encounters. Solid dots are observations and curves are DJL solutions. To agree with DJL solutions, solid dots should fall on curves of the same color.

12
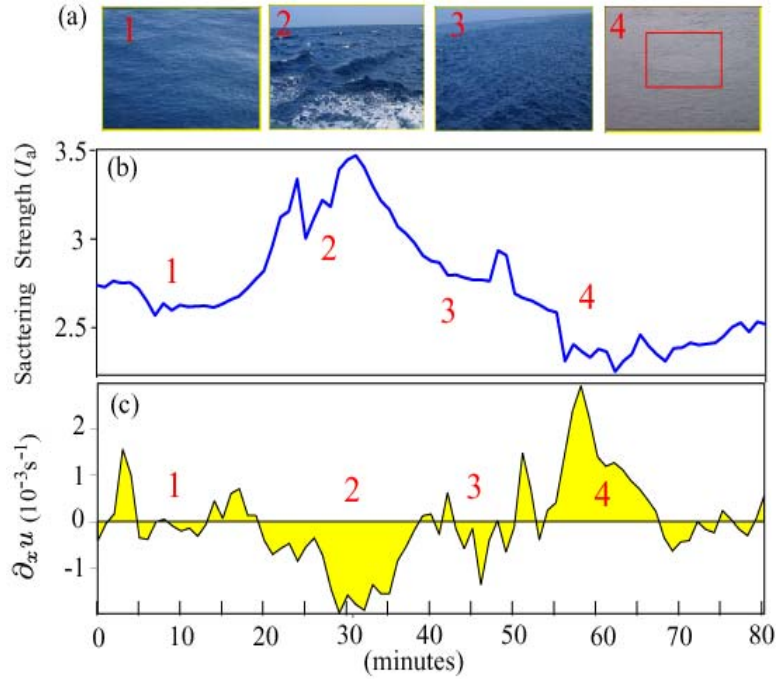
Figure 9: (a) Pictures taken during the experiment illustrating the surface signatures accompanying the passing a NLIW, (b) the marine radar scattering strength, and (c) the horizontal velocity convergence computed from shipboard ADCP measurements in 8.4–12.4-m depth.
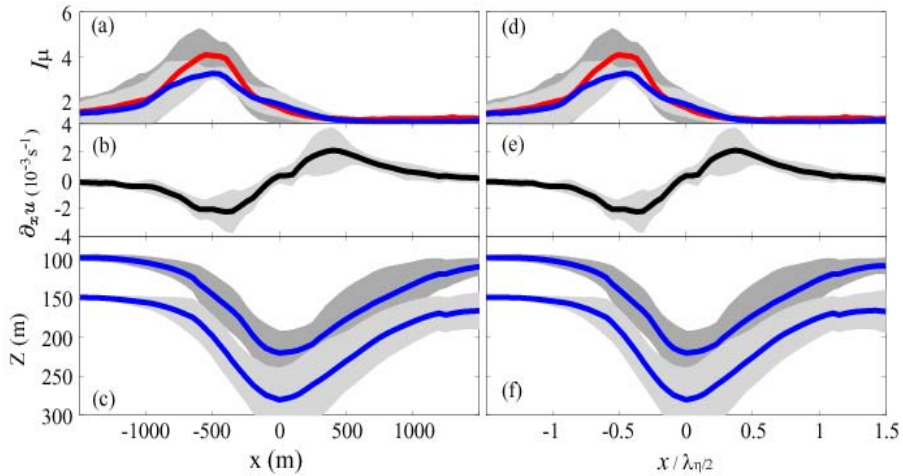
Figure 10: (a) Surface scattering strength, (b) horizontal velocity convergence, and (c) vertical displacement of NLIWs at initial depths of 100 and 150 m averaged over seven NLIW events. (d)–(f) are the same as (a)–(c) except that the x-axis is scaled by the wave width of the half maximum amplitude. Red curves in (a) and (d) represent the surface scattering strength observed from ahead of the propagating NLIWs and the blue curves represent the surface scattering strength observed from behind the propagating NLIWs. The light gray and heavy gray shadings represent 95% confidence intervals.
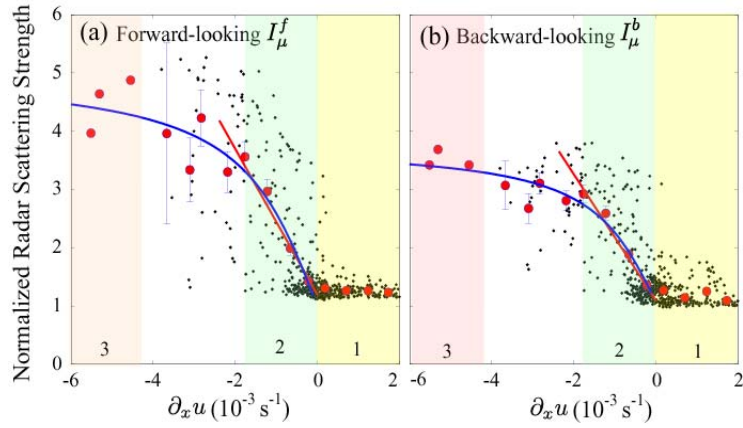
Figure 11: Scatter plots and model fits between the surface scattering strength and the horizontal velocity convergence computed from shipboard ADCP measurements. (a) Observations (gray dots) taken ahead of the propagating NLIWs. Red dots represent averages over constant intervals of horizontal convergence 0.005 s⁻¹. Vertical lines represent 95% confidence intervals. Red and blue curves represent the linear and arctangent fits to observations (red dots). Three regions labeled as 1, 2, and 3 represent the divergence zone, the weak convergence zone, and the strong convergence zone, respectively. Symbols, curves, and labels in the panel (b) are the same as in (a), but observations were taken behind the propagating NLIWs.
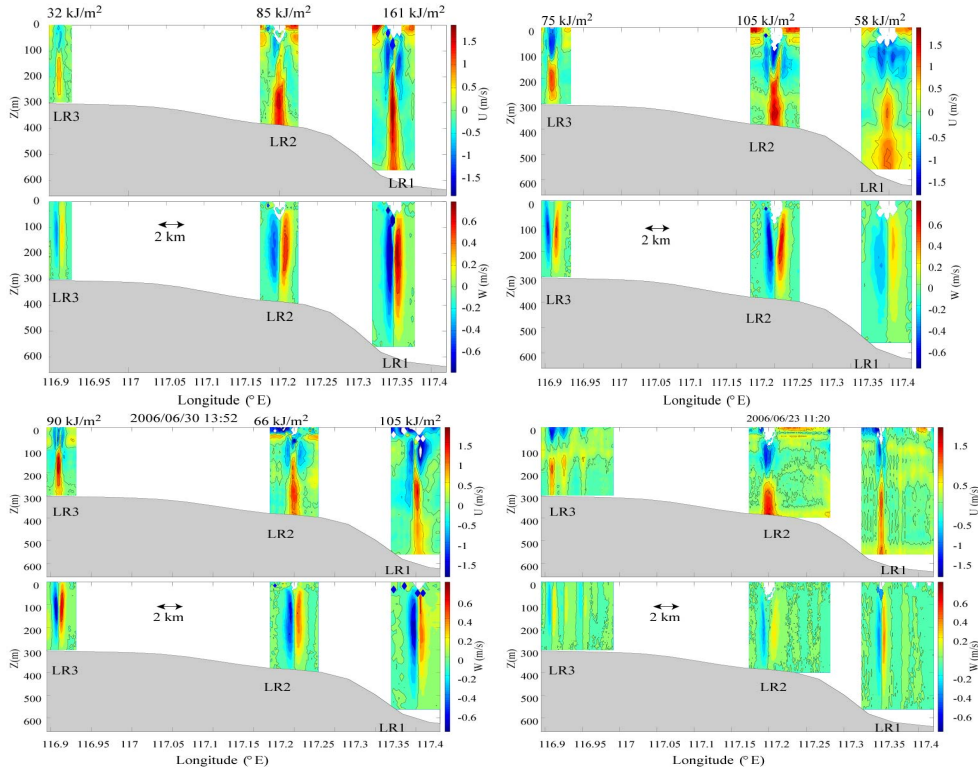
Figure 12: Illustration of the energy evolution of shoaling NLIWs revealed by long-term moored ADCP measurements. NLIWs propagate prevailingly westward. The depth integrated total kinetic energy is shown at the top of panels.

14
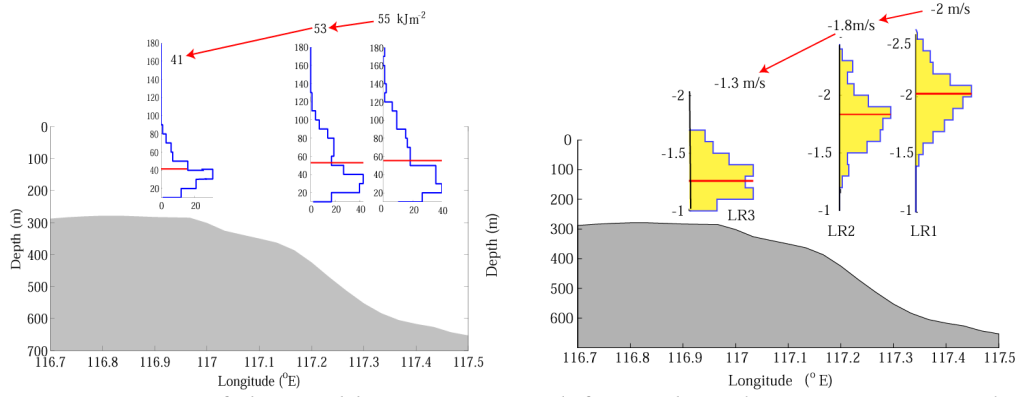
Figure 13: Histograms of the total kinetic energy (left panel) and propagation speed of NLIWs estimated at three mooring sites. Red horizontal lines represent the mean values.
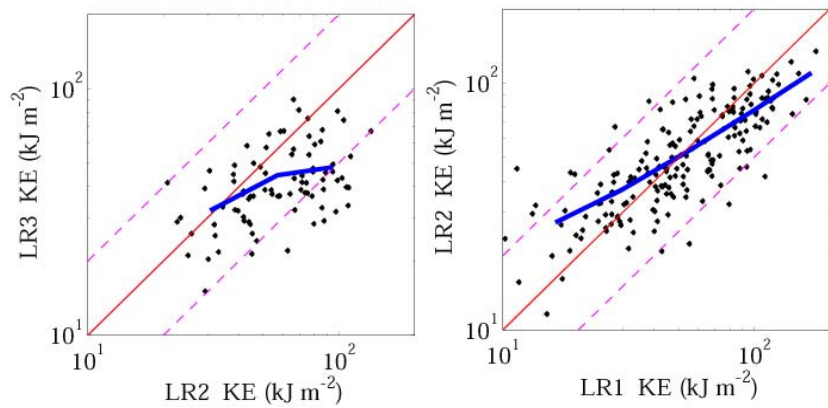

Figure 14: Comparison of the total kinetic energy of NLIWs at three mooring sites. The total kinetic energy is computed after removing the background current (dots). Blue curves are bin averages of black dots.
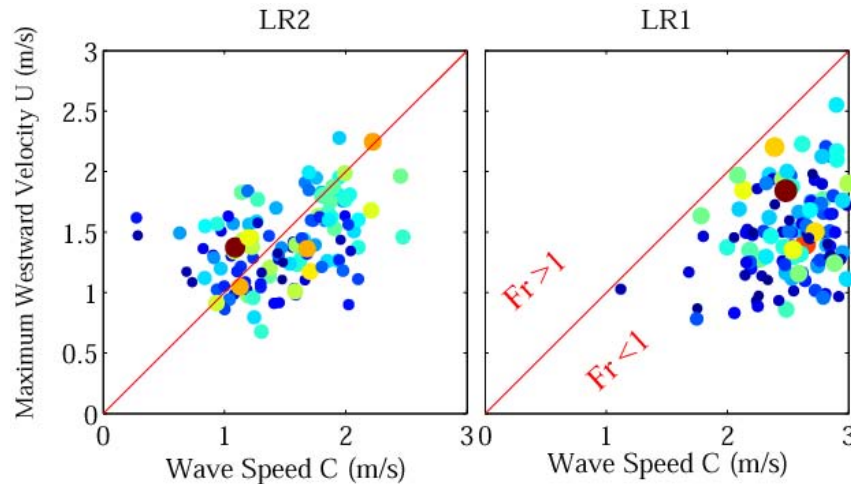

Figure 15: Comparison between the maximum westward velocity and the propagation speed of NLIWs. Colors and sizes of dots represent magnitudes of the total kinetic energy of NLIWs. Red lines indicate $Fr = U_{max}/C = 1$. Trapped cores exists in the region of $Fr>1$.

15
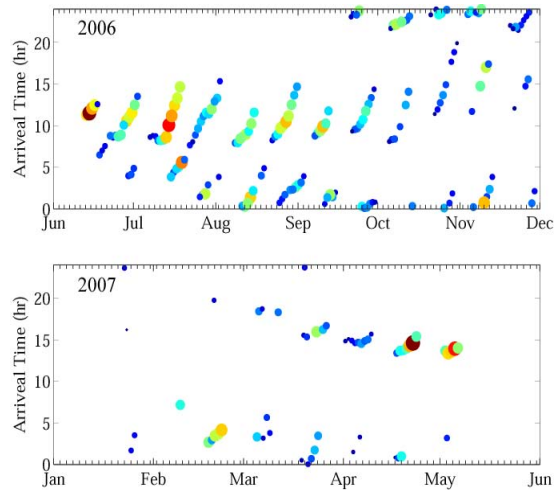
Figure 16: Arrival time of NLIWs in local hour of day at LR1. Sizes and colors of symbols represent the total kinetic energy of NLIWs.
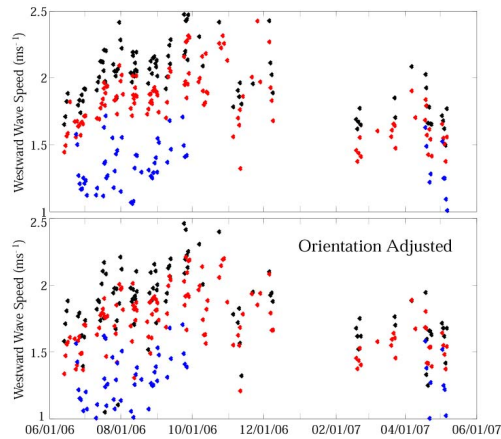

Figure 17: The westward propagation speed of NLIWs (upper panel) and the propagation speed in the wave direction (lower panel). Black, red, and blue dots are estimates of propagation speeds at LR1, LR2, and LR3, respectively.
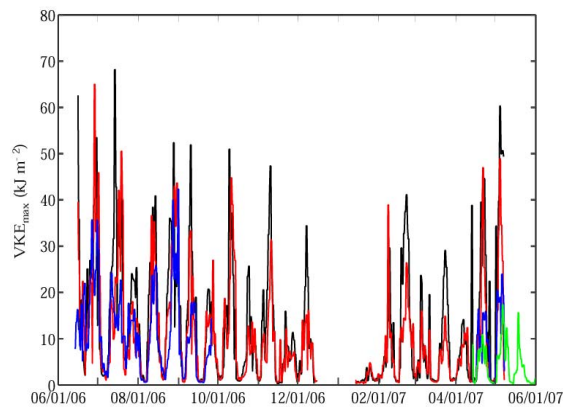

Figure 18: Depth integrated vertical kinetic energy of NLIW. Black, red, and blue curves represent estimates at LR1, LR2, and LR3, respectively.

16
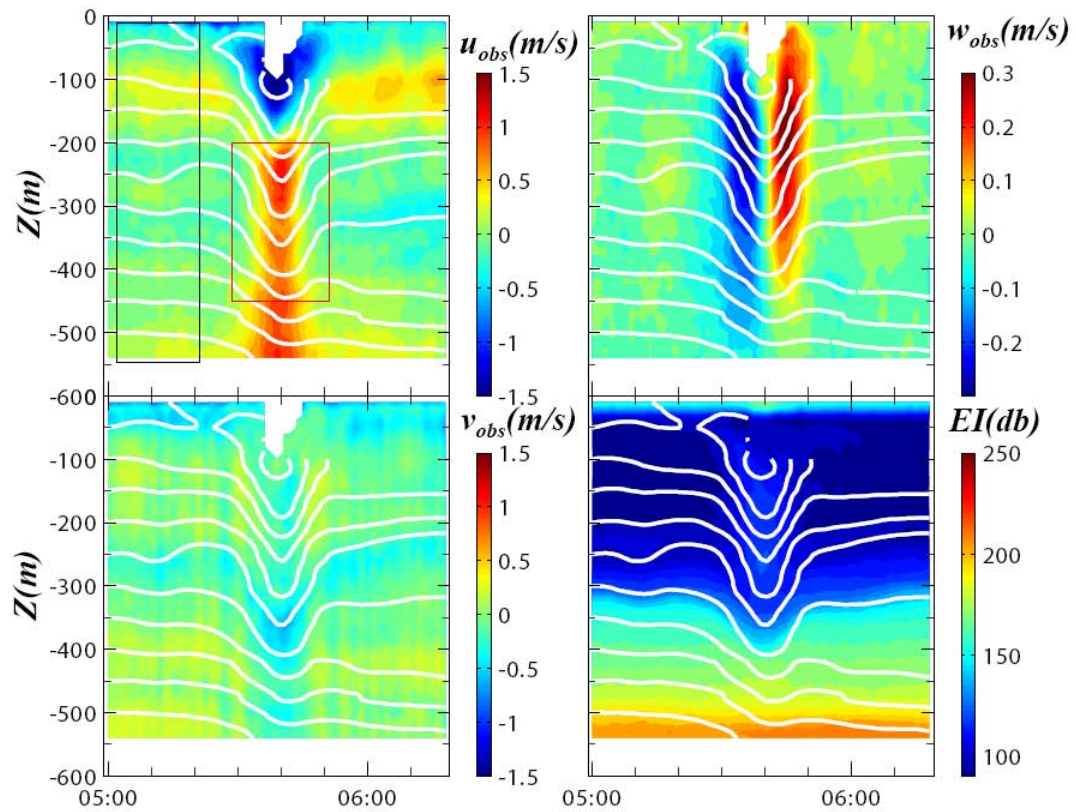
Figure 19: Zonal velocity, meridional velocity, vertical velocity and echo intensity contours of an NLIW event on May 2, 2007. Streamlines are computed using observed vertical velocity. The black box indicates the time interval used to calculate the averaged background flow before NLIW. The red box indicates the time interval and the depth range used to estimate the wave direction and speed.
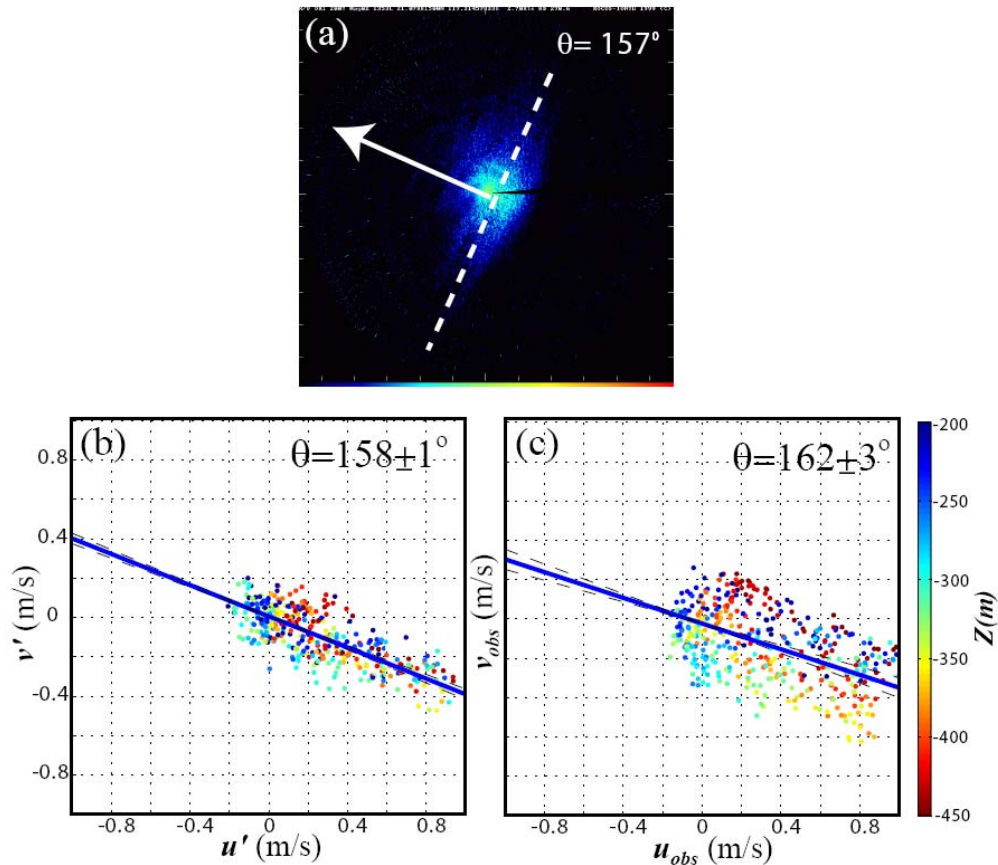
Figure 20: Estimation of propagation direction of NLIWs. (a) Marine radar image of surface scattering intensity induced by NLIWs. (b) The major axis of horizontal velocity, observed on the mooring, of NLIW computed by removing the background velocity field from the observed velocity field following streamlines. (c) The major axis of horizontal velocity observed on the mooring during the NLIW event without subtracting background flow. The propagating direction of NLIW detected by the marine radar is illustrated in (a). The white dashed line shows the NLIW crest and the arrow shows the propagation direction. Color dots in (b) and (c) indicate observations of horizontal velocity at different water depths. Blue solid lines represent the linear least square fit of wave propagation direction. Dashed lines represent their 95% confidence intervals.
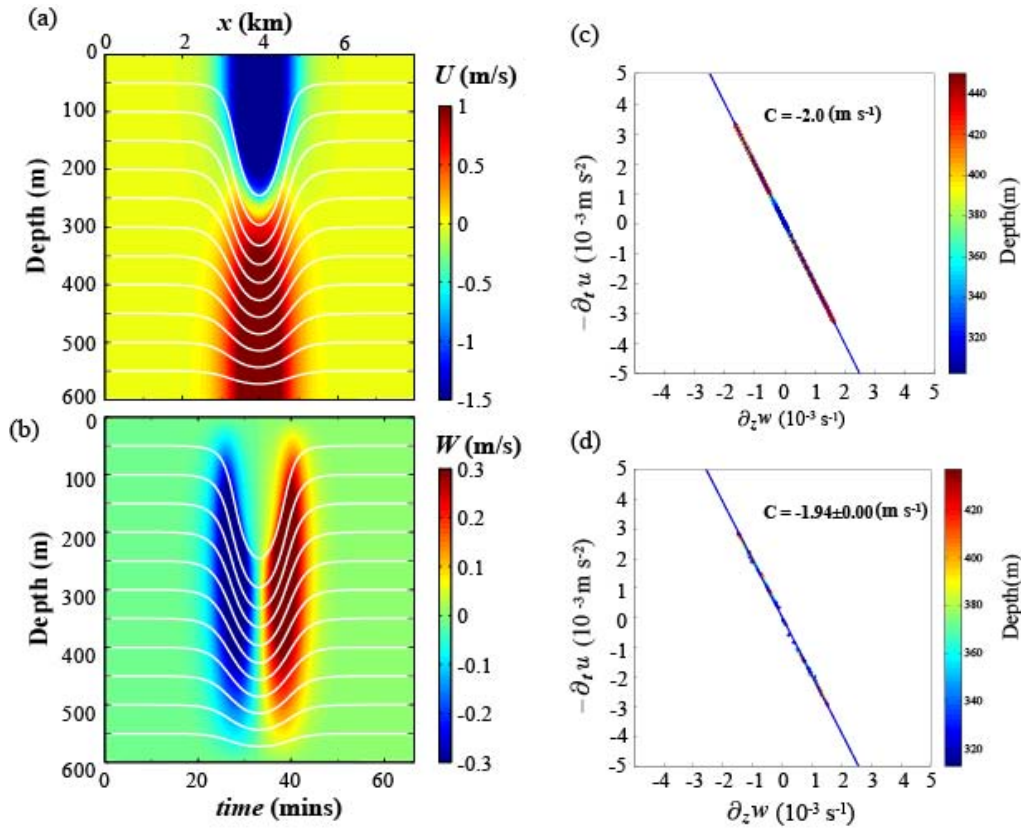
Figure 21: (a) Horizontal velocity and (b) vertical velocity of internal solitary waves simulated by Dubreil–Jacotin–Long (DJL) equation. (c) Scatter plot of the time rate change of horizontal velocity vs. the vertical divergence of vertical velocity at the model spatial grid, ~30 m horizontally (equivalent to ~15 s in time for the wave speed of 2 m s⁻¹) and 2 m vertically. (d) Scatter plot of the time rate change of horizontal velocity vs. the vertical divergence of vertical velocity at a 90-s time interval and 16-m vertical resolution, corresponding to the sampling scheme of our mooring measurements. White curves in panels (a) and (b) represent stream lines. The blue lines represent the slopes derived by the least square method.
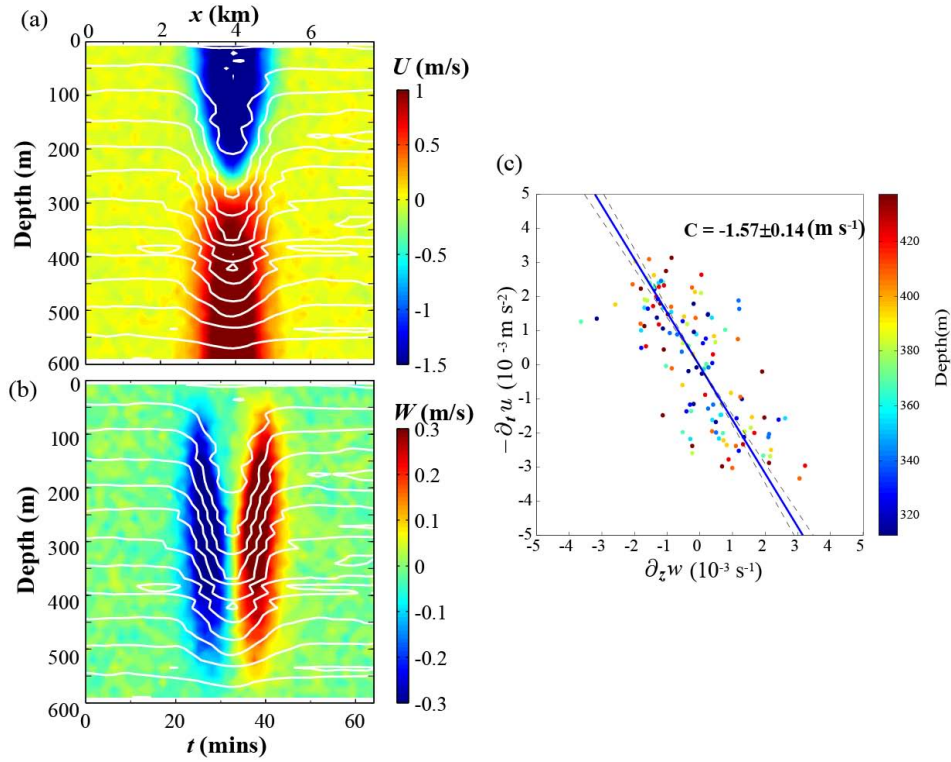
Figure 22: (a) Horizontal velocity and (b) vertical velocity of internal solitary waves simulated by Dubreil–Jacotin–Long (DJL) equation with 0.04 m s⁻¹ random noise in both horizontal and vertical velocity components. (c) Scatter plot of the time rate change of horizontal velocity vs. the vertical divergence of vertical velocity at a 90-s time interval and 16-m vertical resolution, corresponding to the sampling scheme of our mooring measurements. White curves in panels (a) and (b) represent stream lines. The blue lines represent the slope derived by the least square method.
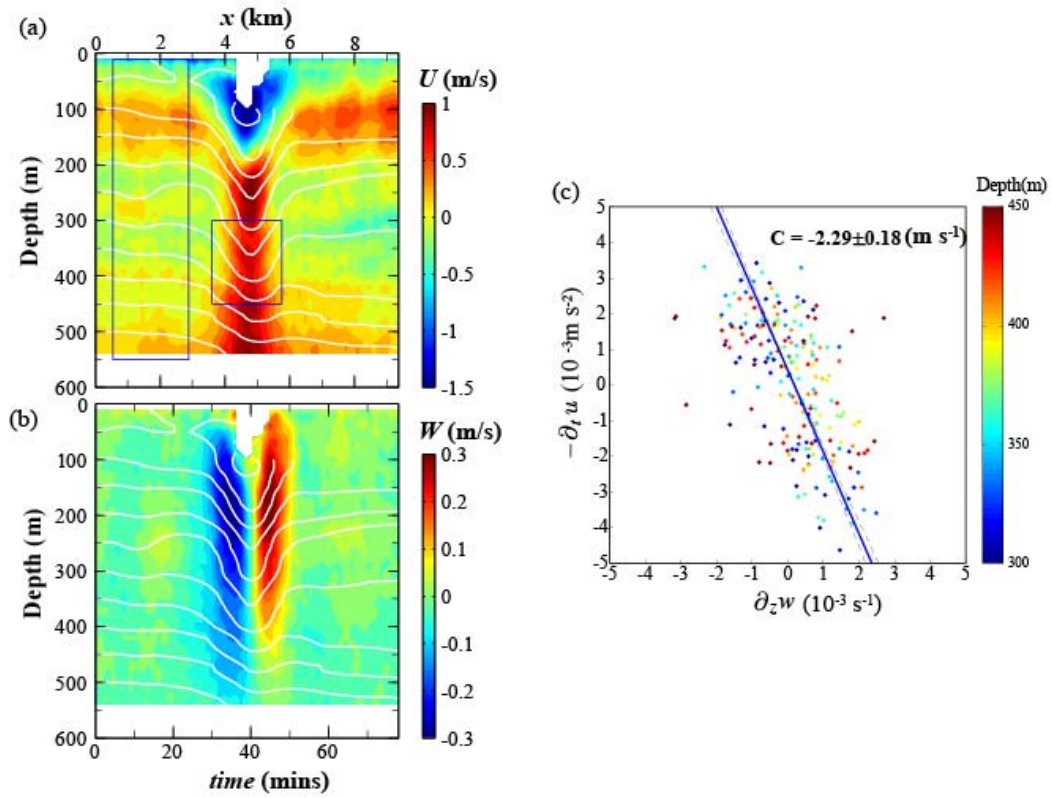
Figure 23: (a) Horizontal velocity and (b) vertical velocity of an observed NLIW event recorded on moored ADCP. (c) Scatter plot of the time rate change of horizontal velocity vs. the vertical divergence of vertical velocity at a 90-s time interval and 16-m vertical resolution. White curves in panels (a) and (b) represent stream lines. The blue lines represent the slope derived by the least square method.

21